International Journal of Science and Research (IJSR)
ISSN: 2319-7064
ResearchGate Impact Factor (2018): 0.28 | SJIF (2018): 7.426

Identification and Restoration of IPMSM Nonlinear EM Characteristics for Motion Control Dynamic Simulation

Kuei-Tsun Chen

11 F-1, No. 69, Longxing St., Banqiao Dist., New Taipei City, 220, Taiwan (R.O.C.)

Abstract: ***This paper is about identifying electromagnetic (EM) nonlinearities of IPMSM using FEM process; specifically, the extracted nonlinear EM elements are restored into dynamic model for variable speed control simulation. And, for the requirement of being closer to actual IPMSM dynamical behavior, non-ideal aspects such as iron-core saturation and cross-saturation between d-/q- magnetic circuits as well as slot-effects should all be included. The former reveals the temporal harmonics, while the later shows the spatial harmonics. Then, the iron loss resistance (R_i) is introduced by correcting the d-/q- equivalent circuit, so as to account for the magnetic losses associated with the above EM nonlinear elements. In this study, data of these nonlinear elements, such as d-/q- inductances (L_d, L_q), BEMF coefficients (K_e) and cogging torque were extracted through FEM software, which are transformed into "Look-Up Table (LUT)" blocks and setup in the dynamic circuit-control model. This nonlinearized model(as Model-III) can be verified by coupling simulation between FEM(2D) and relevant dynamic model(as Model-IV) with "current output/voltage input" method. Besides, through the implementation of this "identification and restoration" process, the simulation time can be greatly reduced from about 24 hours required by Model-IV to only less than 5 minutes for Model-III, and it still keeps close simulation results between the two models.***

Keywords: IPMSM, non-linear EM characteristics, PM, saturation/cross-saturation, temporal/spatial harmonics, d-q inductances, BEMF coefficient, cogging torque, iron-loss resistance, direct-link coupling, current-output/voltage-input

1. Introduction

PMSM is known to be magnetically excited by permanent magnet (PM), and it is capable of using d-q reference frame to develop its mathematical model for Field Oriented Control(FOC) purpose. However, the ideal model is suitable only when the levels of iron-core saturation as well as the cross-saturation between d-q magnetic circuits are very low. For a PMSM based on the linear model considering only constant d-/q-inductances, its control behavior would deviate from expectation of the relevant drive system, and will not be able to reveal actual EM behavior throughout all simulation processes, due to the neglected iron-core saturation as well as the cross-saturation between d-/q-axes magnetic circuits — the "temporal harmonics" of the electromagnetic nonlinearity in the PMSM equivalent circuit. And, for the requirement of being closer to actual PMSM dynamical behavior, non-ideal aspects such as slot-effects, other than the two mentioned, should all be included for simulation[1,2,3]. In this paper, the IPMSM model shown in Fig.(1) is applied for exemplary purpose

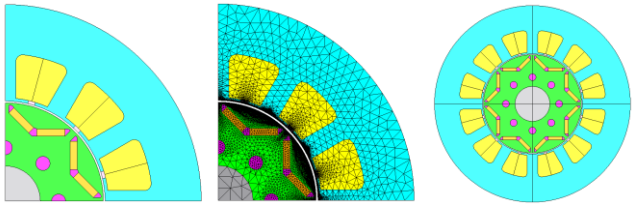

Figure 1: IPMSM (3-phase/8-pole/12-slot) model

Among the non-ideal electromagnetic behaviors, besides the magnetic saturation aspects, there are "spatial harmonics" in the PMSM under no-load (NL) condition (i.e. regardless of current input); and, both the time and space related nonlinear aspects and effects can be explored by FEM package with transient magnetic field analysis mode. More specifically, in terms of the influence of the local geometry and configuration of the motor(such as the stator winding slot, etc.,) the coil flux linkage (λ_{pm}) induced from the PM is not constant, and varies in correlation with the rotary frequency of the machine as shown in Fig.(2). The electromagnetic nonlinear phenomenon caused by spatial geometry is mainly manifested in two aspects: (a) the dynamic torque varying with the rotary angle — cogging torque, and (b) the time-varying rate of the PM flux linkage on the rotor due to the mechanical angular velocity(ω_m) — the voltage effect of no-load BEMF(E_b).

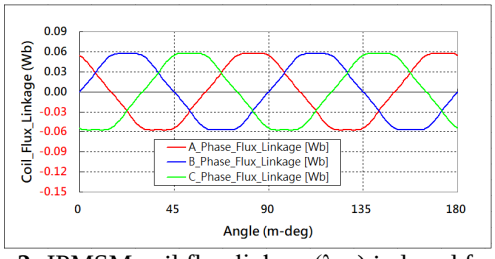

Figure 2: IPMSM coil flux linkage(λ_{pm}) induced from PM under NL condition

From the practical and/or dynamic simulation points of view, in terms of these much detailed and complex electromagnetic phenomena, the numerical model of the IPMSM must be able to approximate the actual features in a close manner whenever

possible, so as to provide the basis for advanced development and design process.

1.1 EM Nonlinearity and Influence in PMSM

In fact, both the magnetic field of the rotor PM and the magnetic field induced by the stator current are constrained by the characteristics of the hysteresis and magnetic saturation of the iron-core. Therefore, if the nonlinear behavior of the iron-core magnetic path is neglected, the response of the dynamic simulation of the motor model will not be consistent with the measured response. Moreover, if an idealized model is applied to the control design, the closed-loop control system will not be able to perform or achieve expected performance. In order to improve the consistency between the measured and the calculated responses of the motor, and to improve the performance of the closed-loop control system, it is necessary to incorporate the nonlinearity of the iron-core into the dynamic model of the electrical machine [4].

In addition, taking IPMSM as an example, the electromagnetic nonlinear elements are all "Zero-Balanced" high-order harmonics superposed on machine's fundamental components of EM quantities, which lead to adverse effects. For example, in terms of time harmonics, the coil current is saturated due to the magnetic circuit and results in Total Harmonic Distortion(THD). In addition, in terms of spatial harmonics, the cogging torque not only fails to provide effective dynamic power, but also causes the mechanical vibration of the drive system, noise, and extra stress load on the machine bearings...etc. Therefore, all of these EM nonlinearities should be reduced to diminish its interference that could obstruct motor operations.

Moreover, the dynamic model can not be used for further simulation and analysis before determining the relevant parameters of the motor. As far as the characteristics of the EM nonlinearity is concerned, different methods applied to obtain the parameters of the PMSM can be summarized into experimental and numerical methods. Based on IPMSM 2-D model as shown in Fig.(1), this study uses FEM software to extract both temporal and spatial non-linear data for detailed dynamic simulations. For temporal aspect, electromagnetic characteristic data(L_d, L_q) is collected to take into account saturation and couple-saturation; and, for spatial portion, curves of BEMF coefficient(K_e) and cogging torque are gathered. The former contains the influence of current and time-dependent characteristics on the magnetic flux linkage, while the later reveals the effect of interaction between the PM and geometry along the air gap. Besides, the above electromagnetic nonlinear factors exhibit fluctuations balanced about fundamental component of EM quantities, so they can be linearly superimposed and consolidated into the d-q equivalent circuit to form a dynamic model, while still suitably follows the same control strategy to actuate the machine based on similar linear design process. In this way, through the modeling environment of circuit-control simulator (e.g., MATLAB/Simulink,) the composition and influence of various electromagnetic nonlinearities can be fully grasped and the simulation results tend to be more realistic.

1.2 PMSM "Field-Circuit-Motion" Coupling

Motor transient "field-circuit-motion" coupling simulation is one of the popular application modes among electromagnetic FEM packages. The process is carried out mainly through the connection between the "internal circuit" of the FEM "field-circuit" model and the "external circuit" of the dynamic model of the circuit/control software(e.g., Simulink). The purpose of such a coupled simulation method is to replace the idealized lumped parameter model with a magnetic field model which takes into account both time and space nonlinear factors as introduced above, such that the combined analysis among magnetic field, circuit, and mechanical motion can fully facilitate the realistic distribution of the magnetic flux within the simulation domain [5,6].

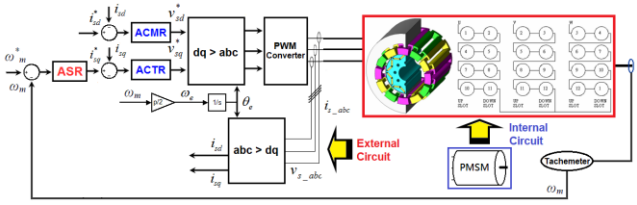

Figure 3: Inner/outer circuits coupling of 'Field-Circuit-Motion'

Moreover, as described above, the external circuit of the motor forms a closed loop with the internal circuit by the feedback mechanism, and the voltage developed by the controller affects the operation of the motor system; however, the motor system has no effect on the controller. This is very close to the operation of a real system, because the control system is always isolated from the controlled target, and this conforms to the coupled mode of simulation between electromagnetic and control sub-systems that can be implemented by numerical methods in the time domain[7]. In this study, the IPMSM model for coupling transient simulations, such as the schematic shown in Fig.(3), includes: (i) the electromagnetic field, (ii) the circuit for transferring external input power to the field, and (iii) the rotor motion that interacts with the field.

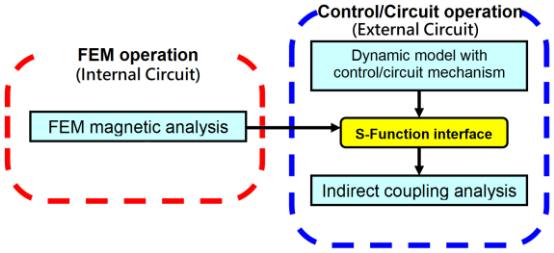

Figure 4: Simulation flowchart of FEM and Simulink coupling

In this study, the indirect coupling is carried out, of which the calculation process is shown in Fig.(4). Usually inside a circuit-control simulator environment, an external interface such as "S-Function" is embedded to extend the functional modules of the FEM software. And, in addition to the parameters(e.g., voltage, current, …, etc.) that are commonly

considered among the relevant equation systems, this interface is also used to couple the two softwares, implement startup/perform numerical solution, and interactively transfer data...etc [8,21].

This paper will be elaborated in the following sequence: in section (B), the formation of electromagnetic nonlinearity in IPMSM is depicted, the characteristics of each nonlinear element is explained, and modifications are outlined based on relevant ideal model; in section (C), the mathematical model of the PMSM is modified by introducing the iron-loss resistance(R_i) into the PMSM equivalent circuit; in section (D), it explains how to collect EM nonlinear parameter data offline by FEM so as to provide real-time dynamic simulation of IPMSM; in Section (E), both the IPMSM non-linearized model(Model-III) and the coupling simulation model (Model-IV) between 2-D FEM and MATLAB/Simulink with "current output/voltage input" method are presented; and, in section (F), validation and feasibility of Model-III is confirmed by comparisons between the simulation results of the two models. Finally, in section (G), the conclusions of this paper are presented.

2. Composition of PMSM EM Nonlinearity

The PMSM temporal and spatial nonlinear factors will affect the magnetic flux distribution of the air gap; in turn, this will also change the motor parameters(L_d, L_q, λ_{pm}, K_e) and the coil winding operating point(current (i_d, i_q) state). Schematics of the magnetic flux distributions in the air gap between linear and nonlinear conditions are differentiated in Fig.(5). In which, (I)-line is the magnetic flux generated by PM only, and (II)-line is the magnetic flux generated by the armature coil only. Accordingly, (III)-line is the total flux that are synthesized by (I) and (II) according to "linear condition"; that is, the effective value of the magnetic flux density on both sides of the PM is equal. On the other hand, (IV)-line is the total flux that are synthesized by "non-linear condition;" in other words, the magnetic flux density on both sides of the N and S poles of PM will have magnetic saturation with the magnitude and the phase angle of the input current.

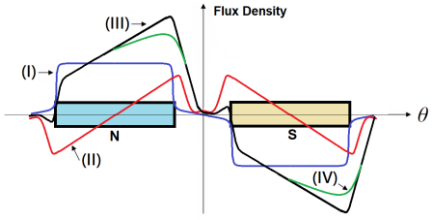

Figure 5: Magnetic flux distribution inside PMSM air gap

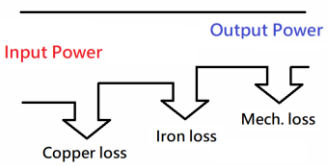

Figure 6: Power flow of PMSM

Moreover, in order to closely approximate the actual magnetic situations of PMSM so as to jump off the ideal linear model being without core-loss assumption, it must follow the power flow of PMSM to comply with the conservation law of energy, as shown in Fig.(6).

2.1 PMSM Nonlinear Characteristics

The phenomenal nonlinearity in the air gap can be further analyzed and decomposed as follows [1,2,3]:

- **Saturated nonlinearity:** The d-/q-flux linkage is magnetically saturated due to current; that is, the synchronous inductances(L_d, L_q) vary with the electromagnetic states(e.g., i_d, i_q amplitude & phase).
- **Coupling nonlinearity:** d-/q-axis magnetic lines share the same magnetic flux path, and there is an interactive saturation effect between the two; and, L_d/L_q are affected by i_d/i_q at the same time, so the total magnetic flux density is not equal to the vector sum of d-/q-components, as depicted in Fig.(5).
- **Spatial harmonic nonlinearity:** The slotting effects vary with the geometrical configuration of the air gap around the motor. The inductance values also vary with local position along circumference.

For the first two items above, the inductances (L_d, L_q) are related to the amplitude and phase of i_d and i_q, while the inductance affected by the third term is related to the spatial geometry of the machine. More specifically, these nonlinearly distributed flux sources exhibit harmonics; in other words, these electromagnetic nonlinear phenomena are accompanied with corresponding iron-losses — magnetic hysteresis loss and eddy current loss.

2.2 Adjustment of PMSM Nonlinear Model

To nonlinearize the IPMSM dynamic model for simulation, the identified nonlinear features extracted from the FEM model can be restored and embodied into the ideal d-q equivalent circuit. An "indetification and restoration" process of EM nonlinear factors is proposed based on following adjustments:

- **Temporal harmonics related to inductances(L_d, L_q) in terms of i_d and i_q amplitude and phase:**
  1) Correct the PMSM equivalent circuit by considering the iron-loss resistance (R_i) which is calculated according to the process proposed in the attached reference [9].
  2) Associate the nonlinear "Characteristic Data" of parameters (L_d, L_q) into voltage equation(Eq.(6)) to demonstrate the magnetic saturations, and is referred to in section (D-1).
- **Spatial harmonics related to the slotting effect:**
  1) Include cogging torque under no-load condition to reveal the influence of local geometrical configuration of the motor, which is referred to in section (D-2).
  2) Associate the BEMF coefficient (K_e) with voltage equation of motion (Eq.(6)) to delineate the effect of PM flux linkage in the air gap that is varied with the spatial angle, which is referred to in section (D-3).

2.3 IPMSM Modified Mathematical Model

Accordingly, in this section, the nonlinear elements of the IPMSM are to be superimposed in the d-q equivalent circuit to form a dynamic model, and the ideal IPMSM mathematical model will be modified to pave for the theoretical basis of the proposed "identification and restoration" process.

2.4 Correction of PMSM Equivalent Circuit

Firstly, the iron-loss resistance(R_i) is added in the linear PMSM equivalent circuit, so that it is parallel to the branches of magnetic excitation and velocity electromotive force, as shown in Fig.(7) [9,10,2]:

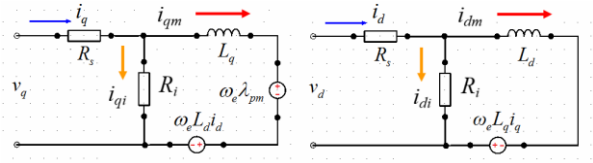

Figure 7: Modified PMSM equivalent circuits

Then, the current components of each branch in the equivalent circuit are estimated according to Kirchhoff's current law, which are listed in Table(1). The i_{di} and i_{qi}(in Eq.(3)) are related to the iron-loss, and their corresponding resistance is represented by R_i; on the other hand, i_{dm} and i_{qm}(in Eq.(4)) are the effective currents actually operating in the windings and related to copper-loss, and the corresponding resistance is R_s. Specifically, the value of R_i is calculated numerically to provide subsequent simulation analysis, which is referred to reference article [9] in details.

Table 1: Current components of each branch in PMSM modified equivalent circuit

$$\begin{cases} i_d = i_{di} + i_{dm} \\ i_q = i_{qi} + i_{qm} \end{cases} \quad (1)$$

$$\begin{cases} \Psi_d = L_d i_{dm} + \lambda_{pm} \\ \Psi_q = L_q i_{qm} \end{cases} \quad (2)$$

$$\Rightarrow \begin{cases} i_{di} = -\dfrac{\omega_e \Psi_q}{R_i} \\ i_{qi} = \dfrac{\omega_e \Psi_d}{R_i} \end{cases} \quad (3)$$

$$\begin{cases} i_{dm} = i_d + \dfrac{\omega_e L_q}{R_i} i_{qm} \\ i_{qm} = i_q - \dfrac{\omega_e L_d}{R_i}\left(i_{dm} + \dfrac{\lambda_{pm}}{L_d}\right) \end{cases} \quad (4)$$

2.5 IPMSM Modified Governing Equations

Table 2: Governing equations of modified PMSM

Voltage equations :

$$\begin{bmatrix} v_d \\ v_q \end{bmatrix} = \begin{bmatrix} R_s & -\omega_e L_q \\ \omega_e L_d & R_s \end{bmatrix} \begin{bmatrix} i_{dm} \\ i_{qm} \end{bmatrix} + \begin{bmatrix} L_d & 0 \\ 0 & L_q \end{bmatrix} \frac{d}{dt} \begin{bmatrix} i_{dm} \\ i_{qm} \end{bmatrix} + E_b \begin{bmatrix} 0 \\ 1 \end{bmatrix} \quad (5)$$

Torque equation :

$$T_{em} = \frac{3}{2} \cdot n_p \cdot \left[\lambda_{pm} i_{qm} + (L_d - L_q) i_{dm} i_{qm}\right] \quad (6)$$

Mechanical motion equation :

$$T_{em} - T_L = J \frac{d\omega_m}{dt} + B\omega_m \quad (7)$$

The modified governing equations of PMSM system can be summarized as in Table(2). Obviously, according to Eqs.(5) and (6), the only two current items that affects the motor governing equations are the i_{dm} and i_{qm}. Thus, the IPMSM dynamic model setup with circuit-control simulator can be considered to meet the conservative-energy law with the inclusion of iron-loss resistance(R_i), which also set the basis for accommodating the EM nonlinear factors to nonlinearize the dynamic model. In addition, according to Newton's second law of motion, Eq.(7) expresses the mechanical movement of the motor associated with output torque(T_{em}), the load of the motor(T_L), friction(B_m) and moment of inertia(J_m) terms.

It is clearly seen that the governing equations of modified PMSM includes all electromagnetic nonlinear features. Among them, the voltage equation contains parameters of inductances (L_d, L_q) and BEMF(E_b). The former is related to the amplitude and phase of i_d and i_q and reveals properties of time harmonics, while the later is related to rotating angle variation and depicts phenomena of spatial harmonics.

3. IPMSM Nonlinear Parameters

With the EM nonlinear characters identified with FEM and restored into a dynamic model of a circuit-control simulator, it is able to reliably predict IPMSM operations for all kinds of dynamic simulations without the cumbersome computational burden required in FEM. In this related research field, experimental and numerical methods are mainly applied to obtain the electromagnetic nonlinear parameters of the motor. In this paper, the parameters of IPMSM inductance characteristic data(L_d, L_q), BEMF(E_b) and cogging torque are obtained only by FEM process.

3.1 PMSM Nonlinear Inductance Data(L_d, L_q)

Corresponding to relevant experimental process, the 'Characteristic Test' is performed under steady-state conditions; that is, the speed of each operating point of the PMSM is kept constant, and a specific current amplitude (Magnitude) and phase angle(Phase) are set. Thus, the operational state of each current group(i_d, i_q) corresponds to an inductance group(L_d, L_q) and a corresponding phase angle. In the FEM environment, the tool exclusively for calculating characteristic inductances of PMSM is applied; then, the result of "current (i_d,i_q)=>(L_d,L_q) inductance" mapping is realized through Excel to form a discrete set of PMSM 'operation data' as shown in Fig.(8).

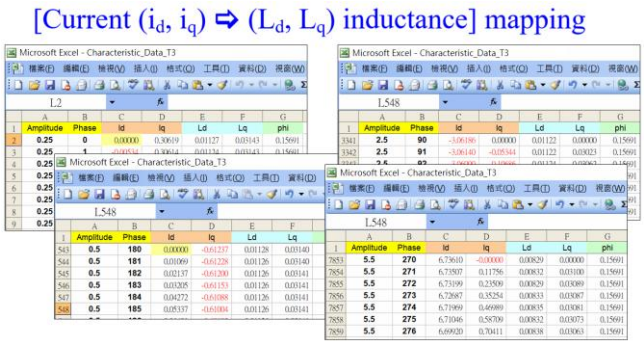

Figure 8: Extraction of IPMSM inductances (L_d, L_q) with FEM

This one-to-one mapping relationship can be used to predict the electromagnetic behavior of PMSM, as shown in Fig.(9)[11]. For each test point, the inductances between the motor d-/q-axes is slightly different due to the nonlinear nature of the motor magnetic flux path(as schematically depicted in Fig.(5)), so the flux linkage of the stator winding is not linearly related with current. Moreover, under fixed current amplitude, the respective inductances (L_d, L_q) vary nonlinearly with different phase angles.

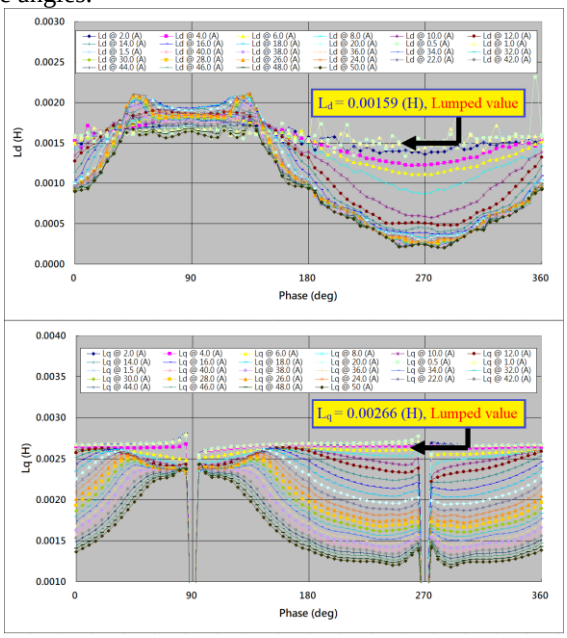

Figure 9: IPMSM inductances (L_d, L_q) analysis show the saturated and coupled nonlinear characteristics

The relevant data can be transformed into Lookup Table(LUT) blocks in Simulink as shown in Fig.(10) [1]. Further, the inductance(L_d, L_q) blocks are to be organized into and associated with Eq.(5) among the items that form the first-order linear differential voltage equation(i.e., the BEMF(E_b) term is excluded for system linearization purpose,) and the "indirect data" modeling is achieved. Moreover, this is a process that utilizes a set of discrete data to approach IPMSM electromagnetic behavior through dynamical interpolation/ extrapolation in real time.

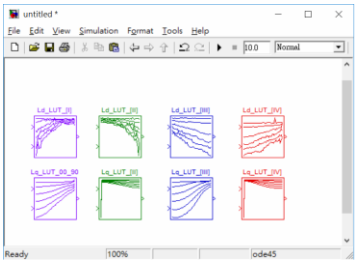

Figure 10: IPMSM inductance LUT blocks

3.2 IPMSM Back EMF Coefficient (K_e)

Inside the voltage equation(Eq.(5)) of the PMSM, under no-load conditions, the BEMF(E_b) of the coil due to time-varying rate of the PM flux linkage(λ_{pm}) can be defined according to Faraday's induction law as shown in Eqs.(8)~(11) [12]. Then, in terms of λ_{pm} distribution waveform, BEMF is intensively conformal to the "imprint" of the geometry along air gap perimeter. And, based on the FEM no-load transient magnetic simulation, the waveform of the BEMF at different speeds is shown in Fig.(11).

$$E_b = \frac{d\lambda_{pm}}{dt} \quad (8)$$

$$E_b = K_e \cdot \omega_m = \lambda_{pm} \cdot \omega_e \quad (9)$$

$$\omega_e = PP \cdot \omega_m \quad (10)$$

$$\lambda_{pm} = \frac{K_e}{PP} = \frac{2 \cdot K_e}{p} \quad (11)$$

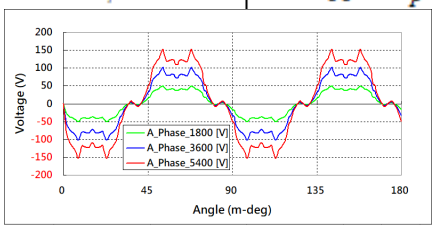

Figure 11: IPMSM BEMF waveform under NL condition

Also, the BEMF coefficient (K_e) can be calculated based on Eq.(10), and a single waveform of K_e is shown in Fig.(12). Obviously, the BEMF coefficient varies periodically with respect to the spatial angle, rather than a constant value as is usually applied in the ideal model. Moreover, from the derivation of Eq.(12), it is concluded that there is a fixed-value proportional relationship between K_e and λ_{pm}. Therefore, during subsequent modeling process, K_e can be used to show the relevant nonlinear features [13].

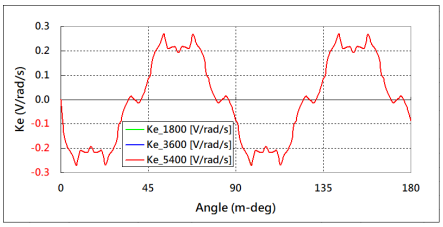

Figure 12: IPMSM K_e waveform under NL condition

3.3 IPMSM Cogging Torque

Nowadays, FEM is much relied on to analyze the EM-forces generated in the magnetic circuit in detail. In general, no matter which method is used to calculate the EM-force in the PMSM, it is necessary to predict the radial and tangential flux densities

in the air gap; and the Maxwell Stress Tensor is usually used under no-load and load conditions, the former condition produces the cogging torque, and the latter is the cause of the torque ripple [14,15].

In terms of physical phenomena, even if there is no current input, the PMSM will alternately produce positive and negative torque about zero-value, which is called "cogging torque". In addition, due to the difference in radial positions between the stator slots and the teeth, the interaction of magnetic fields between the PM and the stator slots causes a tangential force on the stator teeth; and, under NL conditions, this force inclines to 0 — find a position of balancing [16,17,18].

Moreover, with the periodicity of the pitched-geometry of a motor having an integer number of slots, the pattern of the magnetic circuit is repeated depending on the least common multiple(LCM) of the relevant numbers of slots and poles. In this paper, the 8-pole/12-slot IPMSM has a LCM = 24, so the cogging torque shows a period of every 15 degrees, as shown in Fig.(13) [17]. Obviously, this is another geometrical influence of the electrical machine due to the magnetic field distribution, and the smaller the periodical angle the higher order harmonic of this cogging phenomenon.

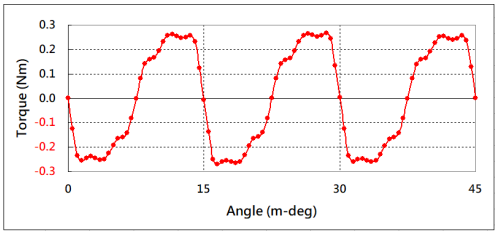

Figure 13: Cogging torque waveform of this IPMSM with a periodicity of 15 degrees

Through the analysis in sections of (D-2) and (D-3), it is known that PMSM electromagnetic nonlinearity is also closely related to the geometrical configuration of the motor and is a function of the circumferential angle(θ). Moreover, both these spatial effects present their own periodical "zero-value" balance, which allow them to be superimposed on the associated torque and voltage equations to form higher order harmonic terms, respectively. Similarly, the BEMF coefficient(K_e) of Fig.(12) and cogging torque of Fig.(13) can be setup as LUT blocks as shown in Fig.(14). Each of the nonlinear blocks is connected with a "position sensor" to output the mapped quantities according to the circumferential angle(θ). Further, under the FOC strategy and based on the voltage "Forward Compensation" method[19], the BEMF coefficient(K_e) block is associated with the voltage equation(Eq.(5)) to reveal the nonlinear characteristics of the BEMF(E_b). On the other hand, the cogging torque LUT block is combined with the EM-torque equation(Eq.(6)) to show the torque ripple under no-load condition.

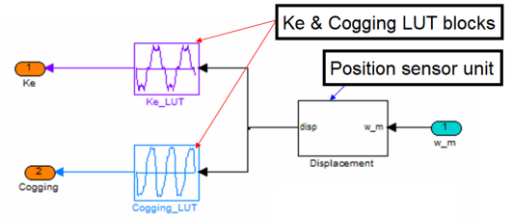

Figure 14: IPMSM K_e and cogging LUT blocks

4. Nonlinearization of PMSM Dynamic Model

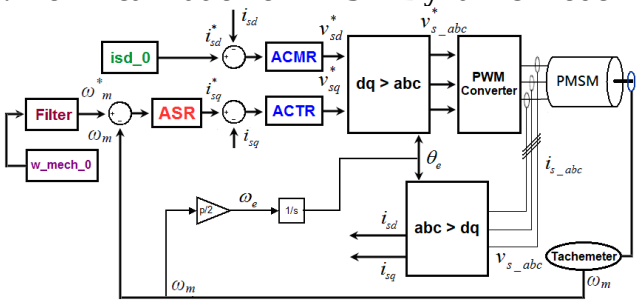

Figure 15: PMSM closed-loop servo-control system with variable frequency PWM converter

Table 3: IPMSM dynamic models in this paper

Models	EM Nonlinear Charactristics		
	Time Harmonics	Space Harmonics	Modified Equivalent Circuit
Model-II	O	X	X
Model-III	O	O	O
Model-IV	FEM(2D)-Simulink coupling		

In this paper, to show and/or compare the characteristics of IPMSM EM nonlinearity, three dynamic models are constructed according to the composing factors listed in Table(3). Among the models, the IPMSM dynamic models are for motion control with the power converter and control units being kept the same as shown in Fig.(15). More specifically, the speed control drive is based on the FOC strategy combined with the constant torque angle(CTA, $i_d = 0$) method. The sine-wave pulse width modulation(SPWM) voltage source inverter(VSI) is applied for the variable frequency power drive. On the other hand, based on the "internal current loop/external speed loop" architecture, a closed-loop control mechanism with PI controllers is used. Besides, the speed controller is further equipped with an anti-integral terminator (Anti-Windup) to overcome the saturation nonlinearity and achieve the robustness of the system control[20,22]. The readers can refer to relevant textbooks and literatures for further details.

4.1 IPMSM Model-II

Model-II is built based on the architecture of the ideal dynamic model and is considering only the nonlinear characteristics of IPMSM magnetic saturations. The "IPMSM" module that characterizes the IPMSM electromagnetic phenomena is shown in Fig.(16); instead of constant inductance values, the nonlinear inductance(L_d, L_q) LUT blocks are sequentially

associated with "Current Calc" and "T_{em} Calc" blocks. And, given the voltage command, the sampling current and the speed, then the d-/q-axis flux linkage can be calculated by Eq.(12), and the electromagnetic torque is calculated by Eq.(6), respectively.

$$\Psi_d = \int \left(v_d - R_s i_d + \omega_e \Psi_q\right) dt$$
$$\Psi_q = \int \left(v_q - R_s i_q + \omega_e \Psi_d\right) dt \quad (12)$$

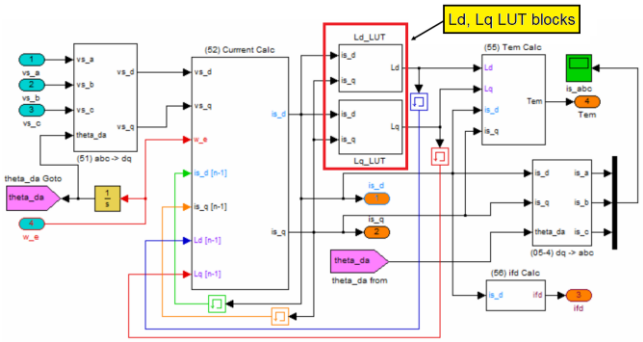

Figure 16: Model-II includes nonlinear inductance LUT blocks

4.2 IPMSM Model-III

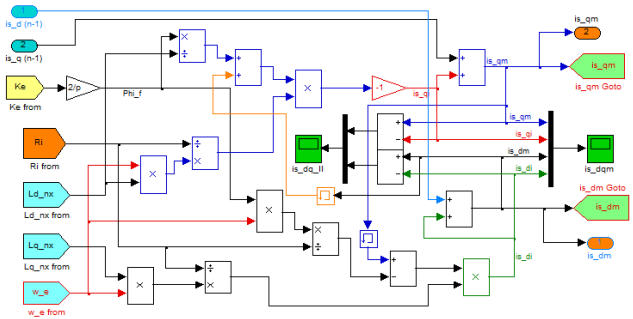

Figure 17: Modified equivalent circuit in the "Current Calc" block

Sequentially, Model-III is generated based on Model-II. In the "Current Calc" module, the equations shown in Table(1) are further utilized to calculate the current components of each branch, as shown in Fig.(17). Since these currents are derived according to the PMSM modified equivalent circuit, the iron-loss of the motor is considered accordingly. In this study, in combination with MATLAB/Simulink, calculation of the iron-loss resistance(R_i) follows the procedure proposed in reference article [9], which is derived by the linear characteristic between Semi-input Power(P_{si}) and Square of Speed Electromagnetic Force (SS_EMF). The slope of this linear relationship corresponds to the reciprocal of the iron-loss resistance($1/R_i$) and is a function of the applied load(T_L) [9]. The R_i result data is collected as shown in Fig.(18), and the relevant data as a function of external load is listed in Table(4). Again, iron-loss resistance can be transformed into a LUT block in Simulink and combined with the mechanical equation of the motor (Eq.(7)) to participate in simulation and analysis, as shown in Fig.(19).

Table 4: IPMSM ironloss resistance(R_i) data list for this study

T_L(Nm)	0	1	2	3	4	5	6	7	8
R_i(Ω)	8.2	6.0	6.0	6.0	5.9	5.9	5.9	6.4	6.2

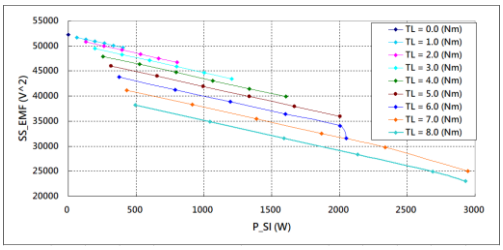

Figure 18: Linear relationship between (P_SI) and (SS_EMF) of IPMSM in this study

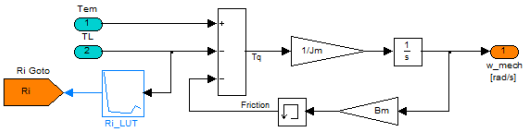

Figure 19: Iron-loss resistance (R_i) LUT is setup with 'EOM' block

4.3 IPMSM Model-IV

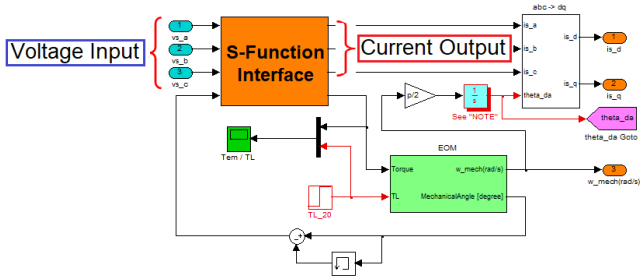

Figure 20: S-function interface is embedded in Model-IV to connect with FEM model of IPMSM

In this study, the Model-IV model is for coupling simulation with the "current output/voltage input" method. And, embedded in the IPMSM dynamic model is a "S-Function" interface connected to an external circuit as shown in Fig.(20). There is a set of output/input ports in the embedded interface for transmitting the voltage/current signals commonly defined between the coupled sub-systems. The phase winding currents (i_a, i_b, i_c) are output from the FEM field solver, which is updated at each time step to reflect the actual operating point of the motor. Simultaneously, the circuit-control simulator solves the phase voltages (v_a, v_b, v_c) according to the associated voltage equation, which are feedback to FEM solver as the input for the next time step. In addition, according to the equation of motion (Eq.(7)) shown in the "EOM" block, the rotor angular position(θ_{disp}) is both an input to the S-function interface and an output value of the "EOM" module. Other output/input data for both sub-systems include electromagnetic torque(T_e), mechanical speed(ω_m), and load torque(T_L).

4.4 IPMSM dynamic simulation analysis

The specifications and parameters of the IPMSM model(as shown in Fig.(1)) as well as the two driving and controlling units are referred to Annex-(1). Simulations of the three models

will be carried out based on the same conditions listed in Table(5). Among the dynamic models, Model-III is the target model proposed in this paper that includes those nonlinear factors identified with FEM. While Model-IV is the same dynamic model generated with circuit-control simulator and is externally coupled with the IPMSM created based on FEM that includes the most comprehensive EM phenomena. Therefore, the output of Model-IV will be used as the benchmark for IPMSM simulation and analysis. Moreover, from the results of Model-II and Model-III, the influence of the modified equivalent circuit considering the iron-loss can be differentiated; in addition, the results compared between Model-III and Model-IV will be used to show how the proposed Model-III can closely approaches the actual electromagnetic phenomena.

Table 5: Simulation conditions of IPMSM

Conditions	Values		Simulation Scenario
Power Freq.	f_n	120 (Hz)	During [0 ~ 0.05 (s)], IPMSM startups from static with empty loading. Then, at t=0.025 (s), the motor overcomes external load and reaches 1800 (rpm) as the steady state speed.
External Load	T_L	1, 2, 4 (Nm)	
Carrier Freq.	f_e	10000 (Hz)	

4.5 Model-II vs. Model-III Simulation Results

A comparison of the simulation results between Model-II and Model-III are shown in Table(6). In general, the waveforms of the two models are similar, but the relevant output quantities differentiate each other to some extents. This is because Model-II includes only the nonlinear inductances(L_d, L_q) without iron-loss resistance(R_i) being considered, and it basically presents behavior of an ideal model at low load(T_L=2 Nm) condition. For example, the three-phase current(i_a, i_b, i_c) is almost a sine-waveform as shown in Fig.(21). Besides, based on the fast Fourier(FFT) analysis as revealed in Fig.(22), fundamental component of Model-III's phase current is 11.5 (%) higher than that of Model-II. This is because the former considers magnetic saturation and accounts for iron-loss. Moreover, with the introduction of electromagnetic nonlinearity, Model-III exhibits distinct fifth and seventh higher order harmonic terms in the current waveforms.

Table 6: Model-II *vs*, Model-III output comparison (T_L = 2 Nm)

	Model-II	Model-III
Speed waveform	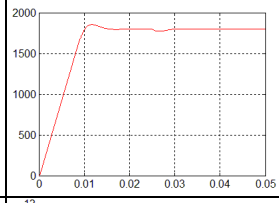	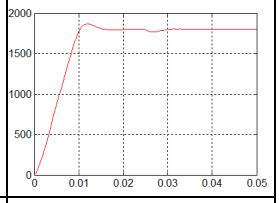
Torque waveform	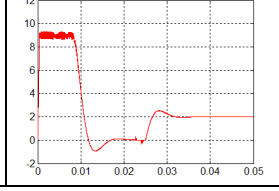	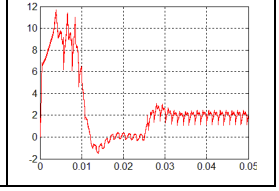

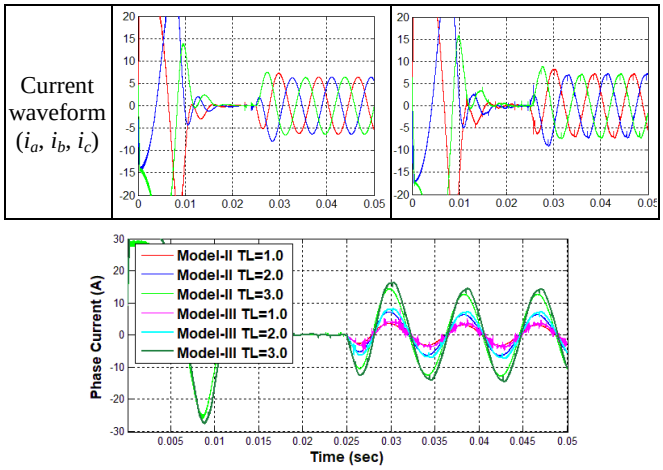

Figure 21: Phase current waveforms comparison at different loads

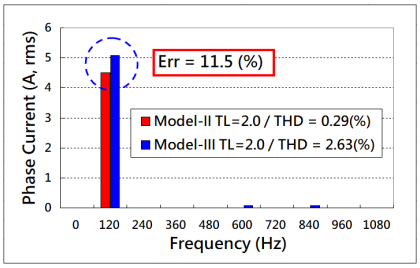

Figure 22: Phase current FFT analysis at T_L=2 Nm

In addition, the spatial nonlinearities(i.e., the cogging torque and the BEMF coefficient(K_e)) are also superimposed within Model-III, so that all the relevant output waveforms present obvious ripples, as shown in Fig.(23). More specifically, during the steady state(0.015 ~ 0.025 [s]) being under no-load condition, it exhibits a cogging torque; while during a steady state(0.03 ~ 0.05 [s]) being subjected to an external load, the torque ripple is dominated by BEMF(E_b) with $T_{em} = i_{qm} \cdot \lambda_m$.

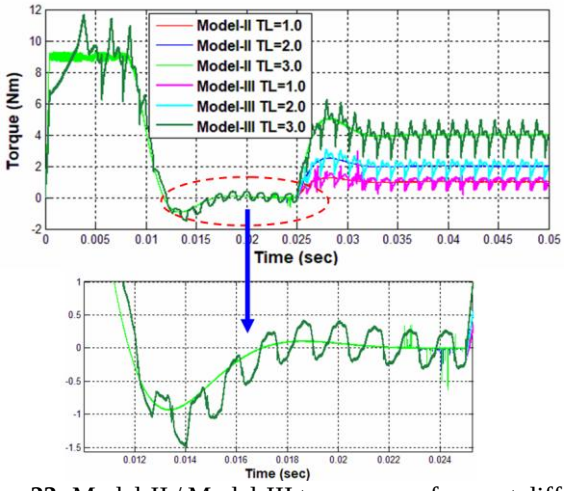

Figure 23: Model-II / Model-III torque waveforms at different loads

4.6 Model-III vs. Model-IV Simulation Results

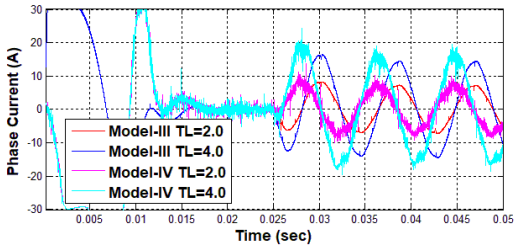

Figure 24: Phase current waveforms comparison at different load

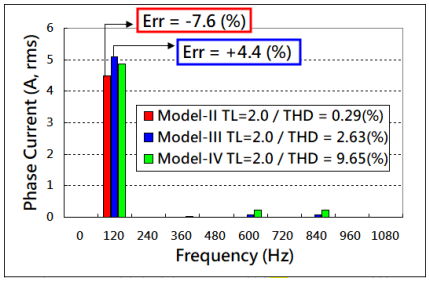

Figure 25: Phase current FFT analysis at T_L=2 Nm

Comparing the three-phase currents under different load conditions as shown in Fig.(24), it is clear that the waveforms of Model-III and Model-IV are similar and their values are close to each other. Also, based on FFT analysis shown in Fig.(25), in contrast to the -7.6(%) error between Model-II and Model-IV, Model-III's current magnitude at fundamental frequency(120 [Hz]) is only 4.4(%) higher than its counterpart of Model-IV. More importantly, both Model-III and Model-IV exhibit prominent fifth and seventh higher harmonic terms. On the other hand, in addition to taking into account the magnetic saturations and iron-loss of modified d-/q-equivalent circuit, Model-III also covers the influence of the geometrical nonlinearities around the air gap(i.e., the characteristics of the spatial harmonics), thus the torque and the rotational speed waveforms are also close to those of Model-IV and exhibit ripples as shown in Fig.(26) and (27), respectively. Therefore, based on the above comparisons of relevant results, Model-III is able to reveal much closer electromagnetic phenomena to those of Model-IV.

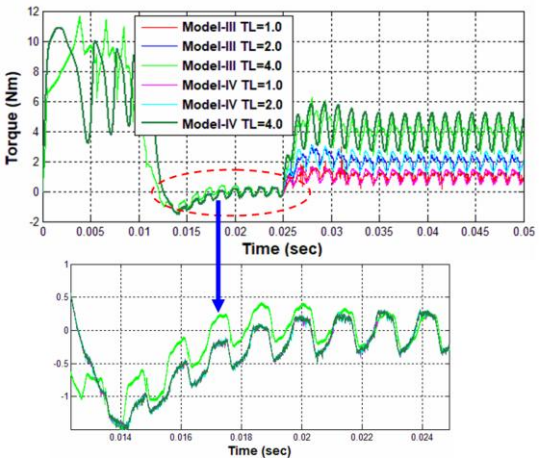

Figure 26: Model-III/Model-IV torque waveforms at different loads

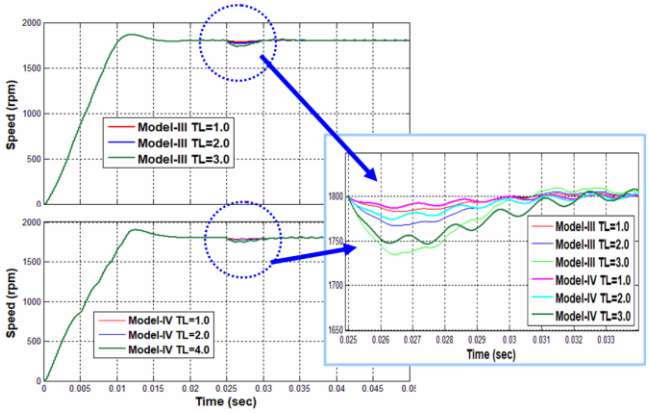

Figure 27: Model-III/Model-IV speed waveforms at different loads

5. Conclusions

Table 7: Time efficiency comparison among IPMSM models

Models	EM Non-linearity			Single Simulation Time
	Time Harmonics	Space Harmonics	Ironloss Resistance	
Model-I	X	X	X	≤ 1 min
Model-II	O	X	X	≤ 3 min
Model-III	O	O	O	≤ 5 min
Model-IV	FEM(2D)-Simulink coupling simulation			~ 1 day

In this study, the electromagnetic nonlinear effects(e.g., inductances(L_d, L_q), BEMF coefficient(K_e), and cogging torque) of an IPMSM are identified using the FEM analyses; then the respective nonlinear phenomena are extracted and consolidated into sets of data. In turn, these discretized nonlinearities are transformed into LUT blocks and restored in the proposed dynamic model of Model-III, which is nonliearized by superimposing those EM nonlinear elements onto the ideal IPMSM dynamic model setup with the circuit-control simulator(like Simulink). And, through the proposed "identification and restoration" process, the EM nonlinearity restored in Model-III can be verified by comparison with the outputs of Model-IV with "current output/voltage input" method. Contribution of this study is that, through the implementation of this "identification and restoration" process, the simulation time can be greatly reduced from about 24 hours required by Model-IV to only less than 5 minutes for Model-III, and it still keeps close simulation results between the two models. Please refer to Table(7) for time efficiency comparison among the three models in this paper.

Also, in terms of using the coupling process of Model-IV to validate the effectiveness of Model-III, the 2-D FEM IPMSM coupled with Simulink model is applied. However, 3-D FEM models like axial-gap PM motors(e.g., Axial-Flux PMSM) is inevitable; and, based on the time-economic considerations, relevant coupling simulation for 3-D FEM model is not effectively applicable with the use of modern commercial computers due to much heavy computation loading. Under such circumstances, as a second contribution, the proposed "identification and restoration" method can provide as a

solution. Please refer to Annex-(2), in which demonstrates a nonlinearized AF-PMSM model based on the proposed process for dynamic simulation. Results of this implementation is concluded in Table (8).

Table 8: Efficacy/efficiency comparison among dynamic simulations of AF-PMSM(3-D) considering EM nonlinearity

FEM(3D)-Simulink coupling process	
Advantage	The magnetic field(FEM) model is used to replace the idealized lumped-parameter model so as to comprehensively cover all the nonlinear aspects. The analysis associated among the magnetic field, circuit and mechanical motion of the motor can faithfully reflect the actual electromagnetic phenomenon of the motor.
Disadvantage	(1) Computer hardware requirements are high, and (2) The numerical calculation time is long; unless it is a "high-speed computer", otherwise the ordinary commercial computer cannot afford such a heavy computation burden.
Proposed "identification and restoration" method	
Advantage	(1) Through the "identification and restoration" process, the temporal and spatial nonlinearities shown in the dynamic model(as demonstrated by Model-III) can capture EM nonlinear characteristic, which is capable of closely reflecting the actual IPMSM operating behavior during the simulation. (2) In the process of modeling, user can understand the composition of various electromagnetic nonlinear factors, and fully grasp the relevant effects for counteracting their adverse influences. (3) Although it takes a longer time to extract L_d & L_q inductance data of the AF-PMSM(3-D), the single dynamic simulation of the nonlinearized model still only needs $\leq$ 5 minutes!
Disadvantage	In the case study, for the 3-D model of AF-PMSM(as shown in Annex-(2), it took 140 hours(about 7 days) to retrieve the (L_d, L_q) data! Even though, it is still worthwhile the effort and time.

References

[1] Thomas Herold, David Franck, Enno Lange and Kay Hameyer, "Extension of a D-Q Model of a PMSM by Saturation, Cross-Coupling and Slotting Effects," Conference Paper, Electric Machines & Drives Conference (IEMDC), May 2011.
[2] Fasil, Muhammed et al, "Improved dq-axes Model of PMSM Considering Airgap Flux Harmonic and Saturation," IEEE Transactions on Applied Superconductivity, 2016.
[3] E. Trancho et al, "IPMSM Torque Control Strategies based on LUTs and VCT Feedback for Robust Control Under Machine Parameter Variations," 42nd Annual Conference of the IEEE Industrial Electronics Society (IECON), 2016.
[4] Gorazd Štumberger et al, "16 Magnetically Nonlinear Dynamic Models of Synchronous Machines: Their Derivation, Parameters and Applications," (Part of the book: New Trends in Technologies), IntechOpen, November, 2010.
[5] Michael Legesse, "Coupled Simulation of an Indirect Field Oriented Controlled Induction Motor Drive," Thesis, Computational Analysis and Design Laboratory, McGill University, Montreal, 2008.
[6] Kuei-Tsun Chen, "Formulation of Transient 'Field-Circuit-Motion' FEM Equations of Induction Machines," Flotrend Co., EM-Newsletter No. FT033, April, 2017.
[7] Kuei-Tsun Chen, "Coupling Simulation Between Electromagnetic FEM and Circuit-Control Sub-systems of Induction Machines," Flotrend Co., EM-Newsletter No. FT034, May, 2017.
[8] Sami Kanerva, "Simulation of Electrical Machines, Circuits and Control Systems Using Finie Element Method and System Simulator," Doctoral Dissertation, Helsinki University of Technology, Espoo 2005.
[9] Naomitsu Urasaki, Tomonobu Senjyu and Katsumi Uezato, "A Novel Calculation Method for Irom Loss Resistance Suitable in Modeling Permanent-Magnet Synchronous Motors," IEEE Transactions on Energy Conversion, Vol. 18, No. 1, March 2003.
[10] Burak Tekgun, "Analysis, Measurement and Estimation of The Core Losses in Electrical Machines," Doctoral Dissertation, University of Akron, December 2016.
[11] Dakai Hu, "Improvement of Torque and Speed Control of PMSM in the Flux-Weakening Region," Doctoral Dissertations, Ohio State University, 2014.
[12] Niranjan Anandrao Patil, "Field Weakening Operation of AC Machines for Traction Drive Applications," Doctoral Dissertations, University of Tennessee - Knoxville, 2009.
[13] Liu Qinghua, "Analysis, Design and Control of PMSM for Wide-Speed Operation," Doctoral Dissertations, National University of Singapore, 2005.
[14] JMAG Division, "JMAG Version 16.1 Reference Manual Volume 1," 6th Edition, JSOL Corporation, March 2018.
[15] Miquel Tost Candel, "Cogging Torque Reduction for Interior Permanent Magnet Synchronous Motors," Master Thesis, Technical University of Darmstadt, 2016.
[16] Engineering Technology Division, JMAG Support Team, "Cogging Torque Analysis of An SPM Motor," JMAG Application Note JAC-040, JSOL Corporation, 2014.
[17] Myeong-Hwan Hwang, Hae-Sol Lee and Hyun-Rok Cha, "Analysis of Torque Ripple and Cogging Torque Reduction in Electric Vehicle Traction Platform Applying Rotor Notched Design," Energies Journal, November, 2018.
[18] Burak Tekgun, "Analysis, Measurement and Estimation of the Core Losses in Electrical Machine," Doctoral Dissertations, University of Akron, 2016.
[19] Kuei-Tsun Chen, "IPMSM Dynamic Simulation of Variable Speed Control Drive Systems," Flotrend Co., EM-Newsletter No. FT028, December, 2018.

[20] Project group: PED4-1038C, "Torque Control in Field Weakening Mode," Master Thesis, Institute of Energy Technology, Aalborg University, June 2009.
[21] Engineering Technology Division, JMAG Support Team, "Iron Loss Analysis of an IPM Motor Accounting for a PWM -Direct Link," JMAG Application Note JAC-059, JSOL Corporation, 2015.
[22] Yi-da Li, "Control System Design and Simulation Using MATLAB/Simulink," Chuan Hwa Publishing Ltd., 2003.

Annexure

Annex-(1) Specification data and system parameters of IPMSM motor for this study

Table 6: IPMSM specification data and system parameters

Items	Symbol / Name		Values
Geometry	stator slots		12
	Stator diameter		112(mm)
	Rotor diameter		56 (mm)
	Air gap width		0.5 (mm)
	Stacklength		65 (mm)
Winding	R_s	Stator resistance	3 (Ohm)
	Stator winding		24 (Turns)
	Wiring		Y-connection
Electrical Specs	p	Pole No.	8
	f_n	Rated frequency	120 (Hz)
	f_c	Carrier frequency	10000 (Hz)
	Power supply (V_{dc})		280 (VDC)
Motor parameters	L_d	d-axis iductance	0.00159 (H)
	L_q	q- axis iductance	0.00266 (H)
	λ_{pm}	PM flux linkage	0.060748 (Wb)
	K_e	BEMF coeff.	0.2707 (Nm/A)
Mechanical parameter	J_m	Inertia	0.00045 (Kgm^2)
	B_m	Friction coeff.	$4.1e^{-5}$ (Nm/deg/s)
Controller parameter	Speed controller	K_P	1.5039
		K_I	945.0319
	Current controller	K_{P_d}	1.8850e+5
		K_{I_d}	99.9026
		K_{P_q}	1.8850e+5
		K_{I_q}	167.1327

Annex-(2) AF-PMSM [Ideal vs. Nonlinear] Dynamic Simulation and EM Characteristics Comparison

A speed control dynamic simulation is for the Axial-flux PMSM as shown in Fig.(Ann-21), and the data and graphs provided herein are to re-enforce the effectiveness and time-efficiency of reproducing the nonlinear EM phenomena of the nonlinearized dynamic model with the same "Identification and Restoration" process proposed in this paper. What is more, although it takes a longer time to extract the nonlinear inductance data(L_d & L_q) of the AF-PMSM(3-D), it is still worth the effort and time because the single dynamic simulation of the nonlinearized model took only less than five minutes!

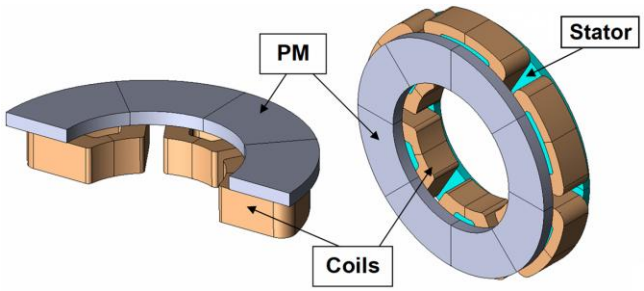

Fig.(Ann-21) 3-D AF-PMSM (3-phase/8-pole/6-slot) model

(a) Extraction of Nonlinear Inductances (L_d & L_q)

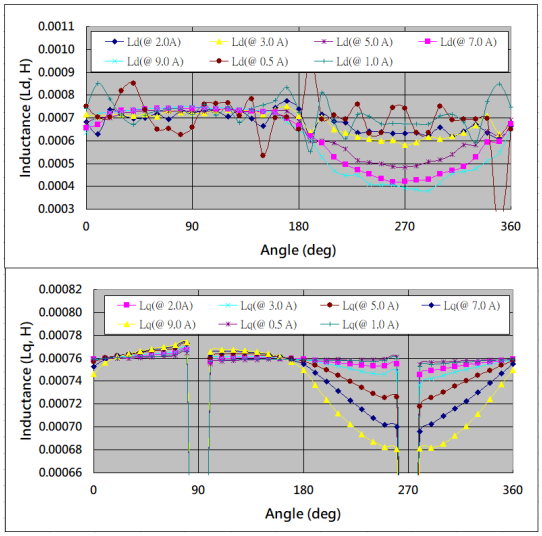

Fig.(Ann-22) AF-PMSM inductances(L_d, L_q)

(b) Analysis of Cogging Torque

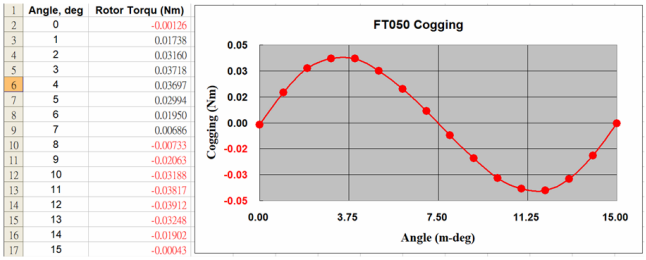

Fig.(Ann-23) Cogging torque of AF-PMSM

(c) Analysis of BEMF Coefficient(K_e)

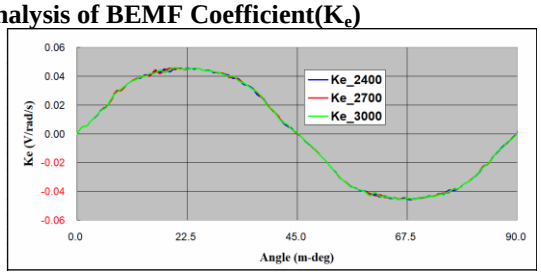

Fig.(Ann-24) AF-PMSM K_e waveform

(d) Result Comparison of [Ideal vs. Nonlinear] Models

Table (Ann-21) Simulation output comparison (T_L = 1 Nm @ 0.02[s])

	Ideal Model	Nonlinear Model
Speed waveform	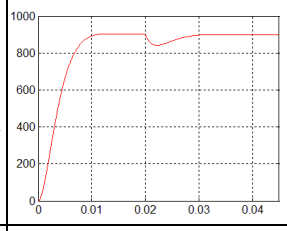	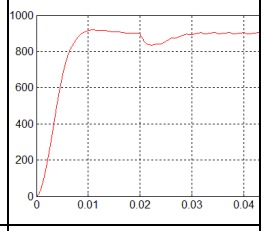
Torque waveform	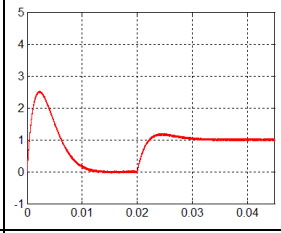	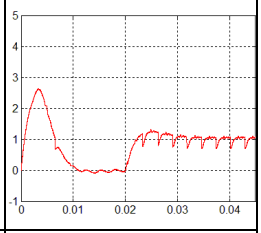
Current waveform (i_a, i_b, i_c)	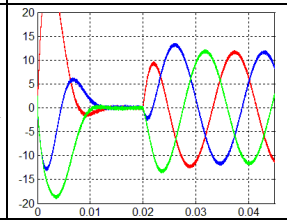	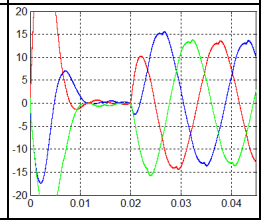

(e) FFT Analysis of Phase Current

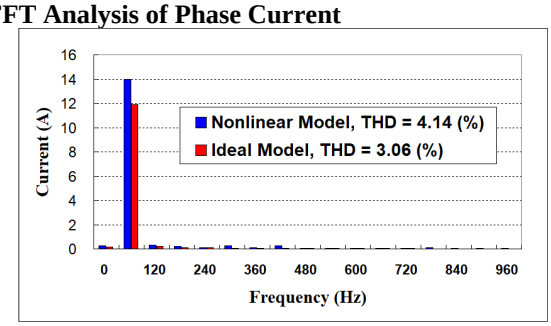

Fig.(Ann-25) FFT analysis of phase current

Author Profile

Kuei-Tsun Chen He received the B.S. degree in Atmospheric Sciences department from National Central University(NCU in Taiwan) in 1986, and received the first M.S. degree in Mechanical and Aerospace Engineering department from CWRU(Ohio, USA) in 1994, and the second M.S. degree in Industrial & Systems Engineering department from USC(California, USA) in 2002. Starting from 1996, he have been serving as a computer-aided(CAD/CAE) application engineer in the industry. He uses thermal/flow, structural, and electromagnetic FEM softwares to help solving customers' problems on interdisciplinary base. For the past fourteen years(2005~2019), he have been dedicated in the electrical engineering field for the simulation and analysis of electrical motors. Currently, he is focusing on the dynamic simulations of AC motors(e.g., PMSM, SynRM, …, etc.,) and is interested in the design of motors with high performance and efficacy.

English abstracts of the Autor's(*Keui-Tsun Chen's*) own reference articles listed in [H. References] of the above submitted manuscript:

[6] Formulation of Transient 'Field-Circuit-Motion' FEM Equations of Induction Machines

This case study extends from the FT032 paper and explores the use of Time-Step FEM to solve the transient magnetic field of an induction motor, and to derive the relevant equation system structure. The electromagnetic field problems of most motors are related to and coupled with electric circuit and mechanical movement. Therefore, when non-sine wave electromagnetic phenomena are considered together with mechanical motion, the time step FEM method is one of the most effective tools for simulating the overall system. In addition, because the system contains ferromagnetic materials, the familiar N-R (Newton-Raphson) method is adopted to deal with related nonlinear problems. In addition, after considering the mechanical motion equation of the motor, the physical position of the rotor will change with time, so the instantaneous position of the rotor is also an unknown variable at each time step. Therefore, it is only after solving the entire coupling equation system can the relevant dynamics. In addition, according to the magnitude of the time constant of each system, the indirect (or weak) method of the "field-path-motion" coupling equation system is one of the general electromagnetic FEM analysis operation modes to simulate the transient magnetic field of the motor.

[7] Coupling Simulation Between Electromagnetic FEM and Circuit-Control Sub-systems of Induction Machines

This study explores a method for coupling a FEM solver with a power electronic circuit-control simulator. Among them, the former's electromagnetic transient model considers the details of the motor geometry configuration and the iron-core magnetic saturation effect; the latter's motor dynamic model includes the PWM power electronics drive circuit and the servo actuation (Servo Operation) Control System. In this integrated simulation environment, by integrating the interaction between the electromagnetic phenomenon of the motor and the control system, it is possible to separately build relevant models, set the coupling between the models, and perform coupling analysis between the two. In this paper, the indirect coupling simulation with the "current output/voltage input" approach method is applied to implement dynamic simulation and analysis of vector control for the three-phase cage induction motor.

[19] IPMSM Dynamic Simulation of Variable Speed Control Drive Systems

This article continues from the FT027 case study and is about the simulation analysis of the steady-state characteristics of IPMSM. First, it is pointed out that the closed-loop servo system of vector control (such as Fig. (4)) can effectively solve the difficulties of starting-up and out-of-step problem for the permanent magnet synchronous motors. Then, the mathematical model is derived for the purpose of implementing the field-oriented control, and the drive control method equivalent to a DC motor are discussed to design the controller of the IPMSM speed servo system. In addition to explaining the basic design concepts of speed and current controllers, the related transfer functions are derived according to PI-type control actions, and the physical phenomena and

functions represented by the closed-loop bandwidth are briefly explained. In this case study, the IPMSM(shown in Fig.(1)) is used as the object, and the self-starting simulation analysis of the rotor with damping winding is carried out in FEM package, circuit-control(e.g., MATLAB/Simulink) simulator is used to simulate the dynamics of the IPM motor performance.